International Journal of Solids and Structures 254–255 (2022) 111899

Contents lists available at ScienceDirect

International Journal of Solids and Structures

journal homepage: www.elsevier.com/locate/ijsolstr

Micropolar beam-like structures under large deformation

Leonid Obrezkov [a,*], Marko K. Matikainen [a], Reijo Kouhia [b]

[a] Mechanical Engineering, LUT University, Yliopistonkatu 34, 53850, Lappeenranta, Finland
[b] Faculty of Built Environment, Tampere University, Korkeakoulunkatu 7, 33720, Finland

ARTICLE INFO

Keywords:
Absolute nodal coordinate
Micropolar continuum
Cosserat continua
Size effect
Micropolar beam
FEM
Cantilever beam

ABSTRACT

Results from experimental torsion and bending tests show the existence of a size effect, which conventional continuum models are unable to describe. Therefore, the incorporation of the micropolar media into numerical approaches for the analysis of materials with a complex microstructure looks necessary. So far, most studies utilize Cosserat continuum theory with 3D finite solid elements, even though, it covers only few beam elements developed within a linear strain–displacement relationship, and therefore only works in a small deformation regime. In this study, the authors aim to develop a size-dependent 3D continuum beam element based on the absolute nodal coordinate formulation (ANCF) with microstructure inclusions. Comparing analytical solutions within the Cosserat continuum model and models based on the proposed and already existing 3D micropolar solid elements, one can see a good correlation between them, with a faster convergence rate for the developed ANCF beam element. That allows exploiting the developed beam element within the non-linear deformation range, which is usually bypassed because of high computational costs, thus, accounting fully for differences between two media descriptions.

1. Introduction

For many decades, bending and torsion tests were widely used in experimental investigations (Liu et al., 2015). However, the material behaviour might differ significantly from the theoretically predicted one because of the microstructure influence (Lakes, 1983; Park and Lakes, 1986). That can come out in various manners, for example, during miniaturization (Lakes, 1986; Engel and Eckstein, 2002), where the so-called size-effect appears. Therefore, the rigidity depends on the object dimensions, and smaller samples respond more stiffly than larger samples from the same material. Current demand for the correct description of miniaturized parts, such as nanostructured materials (Atroshchenko et al., 2017), and the analysis of fibrous materials, e.g., bones (Hassanpour and Heppler, 2017), require the implementation of the microstructure into the modelling process.

One possible way to deal with it is the utilization of extended continuum models, for example, the micropolar (also known as Cosserat) elasticity theory (Carrera and Zozulya, 2021; Neff and Jeong, 2009; Neff et al., 2010). The difference between classical and Cosserat media is in the latter, material particles can be oriented via an additional object called a “director”. Thus, the microrotations associated with points are introduced into the material description. In classical mechanics, a material particle only has one position, and its orientation does not play a role, contrary to the micropolar theory, where the particle orientation influences the results (Pabst, 2005).

The origin of the micropolar continuum theory traces back to the Cosserat brothers’ work (Cosserat and Cosserat, 1909), although its extensive use started after the work of Ericksen and Truesdell (1957), and later, in the 60s, continued wildly internationally (Aero and Kuvshinskii, 1960; Truesdell and Noll, 1965). That progress was then generalized and developed in a number of Eringen’s and Kafadar’s works (Eringen, 1967; Kafadar and Eringen, 1971a,b; Eringen and Kafadar, 1976; Eringen, 1999). Initially designed for viscous fluids, then extended to elastic solids and later applied to the liquid crystal and biomaterial descriptions (Pabst, 2005; Park and Lakes, 1986; Lakes, 1995), the micropolar theory has a variety of applications for materials with a complex inner structure, e.g., fibrous, porous, granular, multilayered materials and molecule polymers (Eremeyev et al., 2016a; Hassanpour and Heppler, 2017; Walsh and Tordesillas, 2006; Riahi and Curran, 2009). Moreover, there is experimental evidence that red cell walls have solid-like elastic properties and can be modelled via Cosserat media (Krishnaswamy, 1996). It can also be applied to the bone description, where size-effect is noted and moments appear in addition to forces (Eremeyev et al., 2016b; Hassanpour and Heppler, 2017), and can provide better results (Lakes, 1986). Thus, this theory is used to overcome the struggle points of classical continuum theories (Carrera and Zozulya, 2021): the size-effects (Neff et al., 2010; Kiani, 2017), problems related to strain localization computations (Ramezani et al.,

* Corresponding author.
E-mail address: Leonid.Obrezkov@lut.fi (L. Obrezkov).

https://doi.org/10.1016/j.ijsolstr.2022.111899
Received 19 April 2022; Received in revised form 29 June 2022; Accepted 20 July 2022
Available online 1 August 2022

2009). All of that is possible because it has additional descriptors for the micromutations and associated with them the internal lengths (Fantuzzi et al., 2018).

From here, one can see the benefits from the inclusion of Cosserat theory into FE modelling. Moreover, it can cure the mesh dependence on FE computations of strain-softening models (Providas and Kattis, 2002; Trovalusci and Masiani, 2003) and stress concentration singularities in contact areas (Eremeyev et al., 2016a). The practical aspects of the implementation can be found in Eremeyev and Skrzat (2017), Ramezani et al. (2009) and Riahi and Curran (2009), where the authors combined the theory with the general 3D continuum FE formulation. Subsequently, the developed element has been applied to numerous problems, even the analysis of beam-like structures (Huang et al., 2000; Tang and Hu, 2017, 2011). However, in these cases, the 3D formulation cannot be considered an efficient solution, and the combination of micropolar theory and beam formulations seems more natural. This combination could be beneficial and have applications in various fields where micro-scaled beam-like structures are taken into account (Kiani, 2017; Akgöz and Civalek, 2015; Atroshchenko et al., 2017; Reddy, 2011): microactuators, micro-electromechanical systems, microsensors, microbiological apparatus, optical microdevices, *etc*. Furthermore, some microstructural biomaterial elements such as struts can be treated as beams, and, therefore, be described with such an element (Eremeyev and Skrzat, 2017). The main possible advantage of the beam formulation is in saving computational power, which is a highly important issue because of the heaviness of the micropolar solid element. Several beam elements based on Euler–Bernoulli, Duleau and Timoshenko theories have been developed in Hassanpour and Heppler (2016) and Nampally and Reddy (2020) to describe the deformation of the micropolar continuum. However, they possess certain limitations as original theories, such as the fixed cross-section in Hassanpour and Heppler (2016). In Nampally and Reddy (2020), the magnitude of microrotation is assumed small with the following accepted approximations, which make them suitable only for small deformation cases. Additionally, the developed elements are utilized within the so-called 2D Cosserat media.

Multibody system (MBS) dynamics offers computer-based approaches to generate and solve the equations of motion of systems of interconnected rigid and elastic bodies. One of them, namely the absolute nodal coordinate formulation (ANCF), was introduced more than two decades ago for highly flexible beam-like structures (Shabana, 1997). The ANCF is a nonlinear finite element approach, where beam elements are represented via continuum-based functions and the number of these functions depends on the necessary level of cross-section deformation description. The key idea behind ANCF-based elements is to use the spatial Hermitian shape functions based on their absolute nodal positions and gradients instead of rotational parameters. The usage of the gradients is a distinguishing feature of ANCF type elements. However, there are several formulations close to it Rhim and Lee (1998) and Choi et al. (2021), which can be considered as variations of this approach. ANCF elements have been applied to standard problems (Nachbagauer, 2014; Ebel et al., 2017) and demonstrated to be more efficient in simple loading cases than the conventional solid elements (Obrezkov et al., 2020, 2021). Additionally, the fairly simple representation of beam-like solid kinematics advocates using this approach (Romero, 2008).

The current work aims to develop a size-dependent beam element by combining an advanced beam formulation and micropolar media. For this reason, the authors have chosen a reliable ANCF continuum-based beam element suitable for torsion and bending tasks and not computationally heavy (Ebel et al., 2017). The micropolar media description for the element is based on the general non-linear formulation presented in Kafadar and Eringen (1971a), which is significantly different from the suppressed number of works within the field where linear material relations are considered. The researchers hope to reveal the possible benefits of the above-mentioned theory and the ANCF combination.

2. Basic relations in micropolar continuum mechanics

Here, we briefly present basic relations of Cosserat continuum theory, which are essential for the next section.

Let $\mathscr{B} \subset \mathbb{R}^3$ be the continuum body at the initial period of time, and we refer to $\bar{\boldsymbol{r}} \in \mathscr{B}$ as a point of the body in the initial configuration. Then we define a smooth function of macrodeformation $\chi : \mathscr{B} \longrightarrow \mathscr{S} \subset \mathbb{R}^3$; therefore, the point position in the actual configuration can be defined as $\boldsymbol{r} = \chi(\bar{\boldsymbol{r}}) \in \mathscr{S}$. We also define two systems of the curvilinear orthogonal coordinate systems $\boldsymbol{x}$ and $\boldsymbol{X}$ corresponding to deformed and undeformed configurations, respectively, with e^i and $\mathscr{E}^i$ covariant base vectors tangent to the coordinate curves, where upper index ^{i} denotes the coordinate's number and takes values 1, 2 and 3. That allows us to define the deformation gradient as

$$\mathbf{F} = \frac{\partial \boldsymbol{x}}{\partial \boldsymbol{X}} = \frac{\partial \chi}{\partial \boldsymbol{X}} = \frac{\partial \boldsymbol{r}}{\partial \bar{\boldsymbol{r}}}, \quad J = \det \mathbf{F} > 0. \tag{1}$$

The micropolar theory takes into account the local rotations of material particles for each point of $\mathscr{B}$. We define the angle of rotation as pseudovector $\boldsymbol{\theta}$. We assume, that in the initial configuration, the microrotation pseudovector is zero vector. Then, the orthogonal micro-rotation tensor has the following form:

$$\mathbf{R} = \exp(\boldsymbol{\Omega}) = \Big(\mathbf{I} + \frac{\sin\theta}{\theta}\boldsymbol{\Omega} + \frac{1-\cos\theta}{\theta^2}\boldsymbol{\Omega}\boldsymbol{\Omega}\Big), \quad \det \mathbf{R} = 1, \tag{2}$$

where $\boldsymbol{\Omega}$ is the skew-symmetric tensor corresponding to $\boldsymbol{\theta}$, having the following representation in the indicial form $\Omega_{ij} = -\varepsilon_{ijk}\theta_k$, θ is the magnitude of $\boldsymbol{\theta}$, and ε_{jmn} are components of the third-order Levi-Civita tensor $\boldsymbol{\varepsilon}$. Eq. (2) presents the so-called the exponential map, which is the common parametrization approach and can be found in Eringen (1967), Kafadar and Eringen (1971a,b), Eringen and Kafadar (1976), Eringen (1999), Ramezani and Naghdabadi (2007), Ramezani et al. (2009), Ramezani and Naghdabadi (2010) and Bauer et al. (2010) *etc.* According to the work (Pietraszkiewicz and Eremeyev, 2009), it is valid in the range $[-2\pi, 2\pi]$, in that work, readers can also familiarize with other ways to parameterize.

In the classical theory, the deformation gradient $\mathbf{F}$ can be uniquely presented via the polar decomposition:

$$\mathbf{F}_c = \mathbf{R}_c\mathbf{U}_c = \mathbf{V}_c\mathbf{R}_c, \tag{3}$$

where $\mathbf{U}_c$ and $\mathbf{V}_c$ are the right and left stretch tensors, respectively, and $\mathbf{R}_c$ is an orthogonal rotation tensor within the classical theory. In the micropolar theory, the deformation measures are defined similarly, as written in Kafadar and Eringen (1971a), but are not the same:

$$\mathbf{U} = \mathbf{F}^T\mathbf{R}, \quad \text{where} \quad \mathbf{F} = \mathbf{R}\mathbf{U}^T. \tag{4}$$

However, the strain measures can be defined in different ways, (see examples in Eringen (1999), Münch et al. (2011) and Eremeyev et al. (2013)). Then, we derive the expression for the wryness or microcurvature tensor $\boldsymbol{\Gamma}$ in the form:

$$\boldsymbol{\Gamma} = -\frac{1}{2}\boldsymbol{\varepsilon} : (\mathbf{R}^T\nabla_{\boldsymbol{X}}\mathbf{R}), \tag{5}$$

where : stands for the double contraction operation and $\nabla_{\boldsymbol{X}}$ is the covariant differentiation operator in the reference coordinate system.

Remark 1. In Eringen's works (Eringen, 1967; Kafadar and Eringen, 1971a,b; Eringen and Kafadar, 1976; Eringen, 1999), the wryness tensor $\boldsymbol{\Gamma}$ expression in Eq. (5) is given only in the index notation. The coordinate invariant form was presented in the works (Ramezani and Naghdabadi, 2007; Ramezani et al., 2009; Ramezani and Naghdabadi, 2010), but it has differences in components between (Ramezani et al., 2009) and Eringen and Kafadar (1976). So, here, to prove our derivation, we present Eq. (5) in the following index notation:

$$\begin{aligned}\Gamma_{ij}e^ie^j &= -\frac{1}{2}\varepsilon_{ilt}e^ie^le^t : (\mathrm{R}_s{}^v e_v e^s \mathrm{R}^{pq}_{,j} e_p e_q e^j)\\ &= \delta_{sp}\frac{1}{2}\varepsilon_{ilt}e^ie^te^l : (\mathrm{R}_p{}^v e_v \mathrm{R}^{pq}_{,l} e_q e^j)\\ &= \delta_{sp}\delta_{tv}\delta_{ql}\frac{1}{2}\varepsilon_{ilt}e^i\mathrm{R}_p{}^t\mathrm{R}^{pl}_{,j}e^j,\end{aligned} \tag{6}$$

where δ_{sp} is the Kronecker delta function and, j denotes the j coordinate differentiation. Hereinafter, we apply the Einstein summation rule over repeating indices. From Eq. (6), one can see that

$$\Gamma_{ij} = \frac{1}{2}\epsilon_{ilt}e^{i}\mathrm{R}_{p}^{\ t}\mathrm{R}_{.j}^{pl},$$

is in complete agreement with formulas given in Eringen's works.

Then, using formula (4), we define the material strain tensor:

$$\mathbf{H} = \mathbf{U} - \mathbf{I}. \tag{7}$$

When restricting to linear kinematics, the material strain and wryness tensors reduce to $\boldsymbol{\epsilon}$ and $\boldsymbol{\kappa}$, respectively, which have the following forms:

$$\begin{aligned} \mathbf{H} &\approx \boldsymbol{\epsilon} = \nabla_{\boldsymbol{X}}\boldsymbol{u}_h^T + \boldsymbol{\Omega} \\ \boldsymbol{\Gamma} &\approx \boldsymbol{\kappa} = \nabla_{\boldsymbol{X}}\boldsymbol{\theta}, \end{aligned} \tag{8}$$

where the translation $\boldsymbol{u}_h$ field is defined as follows:

$$\boldsymbol{u}_h = \boldsymbol{r} - \bar{\boldsymbol{r}}. \tag{9}$$

where the second one is responsible for the moment description interactions (Eremeyev et al., 2016a), or in component form as:

$$\begin{aligned} \epsilon_{ij} &= u_{h_{j,i}} - \varepsilon_{ijk}\theta_k, \\ \kappa_{ij} &= \theta_{i,j}, \end{aligned} \tag{10}$$

As it is possible to see from (10), even in a geometrically linear case, the strain tensors are not symmetrical. Additionally, we would like to draw the attention of our readers to the expressions of (10) – especially to the index order of the of Levi-Civita tensor components and the component order of the rotational field differentiation.

In this work, we consider a linear isotropic micropolar solid, where the relations between stress $\mathbf{t}$ and couple stress $\mathbf{m}$ tensors and the material strain and wryness tensors are:

$$\begin{aligned} \mathbf{t} &= \lambda\mathrm{tr}(\mathbf{H})\mathbf{I} + (\mu + k)\mathbf{H} + \mu\mathbf{H}^T, \\ \mathbf{m} &= \alpha\mathrm{tr}(\boldsymbol{\Gamma})\mathbf{I} + \beta\boldsymbol{\Gamma} + \gamma\boldsymbol{\Gamma}^T. \end{aligned} \tag{11}$$

It can also be written in a compact form as Pabst (2005), Eremeyev et al. (2016a) and Eringen and Kafadar (1976):

$$\begin{aligned} t_{ij} &= \overline{C}_{ijkl}\epsilon_{kl}, \\ m_{ij} &= \tilde{C}_{ijkl}\kappa_{kl}, \end{aligned} \tag{12}$$

where $\overline{C}_{ijkl}$ and $\tilde{C}_{ijkl}$ are the elasticity tensors, which in the isotropic case can be written as:

$$\begin{aligned} \overline{C}_{ijkl} &= \lambda\delta_{ij}\delta_{kl} + (\mu + \kappa)\delta_{ik}\delta_{jl} + \mu\delta_{il}\delta_{jk}, \\ \tilde{C}_{ijkl} &= \alpha\delta_{ij}\delta_{kl} + \beta\delta_{ik}\delta_{jl} + \gamma\delta_{il}\delta_{jk}. \end{aligned}$$

The six elastic constants: $\lambda, \mu, \kappa, \alpha, \beta, \gamma$ should satisfy the following conditions in order to meet the postulate of thermodynamic stability (Eringen, 1999):

$$\begin{aligned} 3\lambda + 2\mu + \kappa &\geqslant 0, \\ 2\mu + \kappa &\geqslant 0, \\ \kappa &\geqslant 0, \\ 3\alpha + \beta + \gamma &\geqslant 0, \\ \gamma &\geqslant \beta \geqslant -\gamma. \end{aligned} \tag{13}$$

The linear elastic constitutive equations can be written in slightly different forms, which can cause confusion when comparing the results (Carrera and Zozulya, 2021). Important work to clarify this ambiguity has been done by Hassanpour and Heppler (2017), summarizing five different notations. Additionally, the elastic constants can be presented in the form of technical parameters (Eremeyev et al., 2016b; Lakes, 1995):

$$G = \frac{2\mu + \kappa}{2}, \quad \nu = \frac{\lambda}{2\lambda + 2\mu + \kappa}, \quad l_t^2 = \frac{\beta + \gamma}{2\mu + \kappa},$$

$$l_b^2 = \frac{\gamma}{2(2\mu + \kappa)}, \quad N^2 = \frac{\kappa}{2(\mu + \kappa)}, \quad \Psi = \frac{\beta + \gamma}{\alpha + \beta + \gamma},$$

where G is the shear modulus, ν is Poisson's ratio, l_t is the characteristic length for torsion, l_b is the characteristic length for bending, N is a coupling number and Ψ is the polar ratio. As can be seen, there are two length scales. Interesting advice related to these length scales is given in the work (Atroshchenko et al., 2017): the relationship between the size of the Cosserat intrinsic length scales and the size of the material sample $l_t, l_b \ll L$ leads to the standard theory; in the case $l_t, l_b \approx L$, the bodies should be approximated by the micropolar media.

In this work, the technical parameters are used. However, if in the references have, as for example in Huang et al. (2000) and Tang and Hu (2017), different notations, the material parameters are transformed to the technical ones.

It is possible to reduce the number of elastic coefficients to four by requiring, conformally invariant curvature state (Neff and Jeong, 2009; Neff et al., 2010). As a result, the micro-curvature tensor is symmetric, resulting in the symmetric moment stress tensor. Yang et al. (2002) and Surana et al. (2017) have postulated an additional balance equation, which also yields the symmetric moment stress tensor. In the conformally invariant curvature state, $\gamma = \beta$, $\beta = \mu l_t^2$ and $\alpha = -\frac{2}{3}\mu l_t^2$. In addition to the reduction of the number of material parameters, the conformally invariant curvature assumption results in bounded stiffness when the size of the object tends to zero.

From the balance equations of linear momentum and the moment of momentum, the equilibrium equations can be obtained in the following form:

$$\begin{aligned} \nabla_{\boldsymbol{X}} \cdot \mathbf{t} + \boldsymbol{f} &= \boldsymbol{0}, \\ \nabla_{\boldsymbol{X}} \cdot \mathbf{m} + \boldsymbol{\varepsilon} : \mathbf{m} + \boldsymbol{c} &= \mathcal{O} \end{aligned} \tag{14}$$

or in the component form:

$$\begin{aligned} t_{ij,i} + f_j &= 0, \\ m_{ij,i} + \varepsilon_{jmn}t_{mn} + c_j &= 0 \end{aligned} \tag{15}$$

where t_{ij} and m_{ij} are components of the stress $\mathbf{t}$ and couple stress tensors $\mathbf{m}$, respectively. Finally, f_i and c_i are the components of external body forces and couples $\boldsymbol{f}$ and $\boldsymbol{c}$.

Thus, with the above-mentioned expressions, it is possible to describe the deformation mechanism of the micropolar isotropic linear elastic continuum. However, even for such a micropolar media case, there are a few publications, where data for the elastic constants given.

3. ANCF element for micropolar media

In this section, we describe the kinematics of a beam element. We focus our attention on continuum-based ANCF elements due to their ability to faithfully represent the deformations of slender bodies and incorporate constitutive models without any modification (Romero, 2008).

Before we present our approach in detail, we would like to explain the reason for this choice. The ANCF elements were already used for various applications and showed results in good agreement with the references. They also demonstrate better convergence rates against the commercial software solutions (Obrezkov et al., 2020). However, some beam elements, despite their benefits, have weak points: for example, suffering from various locking phenomena. Assuming in advance that the size-effect reveals itself during bending and has a significant influence on it Liu et al. (2015) and Engel and Eckstein (2002), it is reasonable to choose the element that has no additional problems with this type of deformation.

Among all variations of the ANCF continuum-based beam elements, we limit our choice to the three-noded high-ordered ANCF beam element called 3363c. The reason is based on the work of Ebel et al. (2017), where it was finalized that only this element gives appropriate results in all conducted nonlinear tests and maintains a reasonable

convergence rate. Also, it does not require any curing modifications for better performance (Obrezkov et al., 2022). To distinguish the element dealing with Cauchy-continua, it will in this work be referred to as "ANCF Cauchy". The element applied to the micropolar media description, we call "ANCF Cosserat".

The whole procedure for the ANCF Cosserat element is similar to the ANCF Cauchy one. As was already mentioned, the micropolar elasticity utilizes alongside displacement components three microrotation degrees of freedom. Here, we apply to the microrotation field the same approximation procedure as to the displacement vector field, with the same shape functions. Then, the whole shape function matrix has the following form:

$$\mathbf{N}_m(\xi,\eta,\zeta) = \left[N_1\tilde{\mathbf{I}}\ \ N_2\tilde{\mathbf{I}}\ \ N_3\tilde{\mathbf{I}}\ \ \ldots\ \ N_{18}\tilde{\mathbf{I}}\right], \tag{16}$$

where $\tilde{\mathbf{I}}$ is an 6×6 identity matrix, and shape functions can be written as:

$$N_1 = \frac{1}{2}\xi(\xi-1) \qquad N_2 = \frac{1}{4}l_y\xi\eta(\xi-1) \qquad N_3 = \frac{1}{4}l_z\xi\zeta(\xi-1)$$

$$N_4 = \frac{1}{8}l_z l_y\xi\eta\zeta(\xi-1) \qquad N_5 = \frac{1}{16}l_y^2\xi\eta^2(\xi-1) \qquad N_6 = \frac{1}{16}l_z^2\xi\zeta^2(\xi-1)$$

$$N_7 = 1-\xi^2 \qquad N_8 = \frac{1}{2}l_y\eta(1-\xi^2) \qquad N_9 = \frac{1}{2}l_z\zeta(1-\xi^2)$$

$$N_{10} = \frac{1}{4}l_z l_y\eta\zeta(1-\xi^2) \qquad N_{11} = \frac{1}{8}l_y^2\eta^2(1-\xi^2) \qquad N_{12} = \frac{1}{8}l_z^2\zeta^2(1-\xi^2)$$

$$N_{13} = \frac{1}{2}\xi(\xi+1) \qquad N_{14} = \frac{1}{4}l_y\xi\eta(\xi+1) \qquad N_{15} = \frac{1}{4}l_z\xi\zeta(\xi+1)$$

$$N_{16} = \frac{1}{8}l_z l_y\xi\eta\zeta(\xi+1) \qquad N_{17} = \frac{1}{16}l_y^2\xi\eta^2(\xi+1) \qquad N_{18} = \frac{1}{16}l_z^2\xi\zeta^2(\xi+1).$$

ξ,η,ζ are the bi-normalized coordinates in the local coordinate system $\boldsymbol{\xi}$ with the range $[-1,1]$; l_x, l_y and l_z are the physical dimensions of the element. Assuming that for the ith node we have the following set of the nodal coordinate $\boldsymbol{q}_i$ (see Fig. 1):

$$\boldsymbol{q}_i = \left[\boldsymbol{r}^{iT}\ \boldsymbol{r}^{iT}_{,y}\ \boldsymbol{r}^{iT}_{,z}, \boldsymbol{r}^{iT}_{,yy}\ \boldsymbol{r}^{iT}_{,yz},\ \boldsymbol{r}^{iT}_{,zz}, \boldsymbol{\theta}^{iT}\ \boldsymbol{\theta}^{iT}_{,y}\ \boldsymbol{\theta}^{iT}_{,z}\ \boldsymbol{\theta}^{iT}_{,yy}\ \boldsymbol{\theta}^{iT}_{,yz}\ \boldsymbol{\theta}^{iT}_{,zz}\right]^T, \tag{17}$$

Hence, instead of the general curvilinear orthogonal coordinates, we use Cartesian systems. Therefore, shorthand symbols used in Eq. (17) are:

$$\boldsymbol{r}^i_{,\alpha} = \frac{\partial \boldsymbol{r}^i}{\partial\alpha},\ \alpha = \{y,z\}. \tag{18}$$

Then, the finite element approximation can be expressed in the form:

$$\{\boldsymbol{r},\boldsymbol{\theta}\} = \mathbf{N}_m(\xi,\eta,\zeta)\,\boldsymbol{q}(t). \tag{19}$$

With (19), the expressions for (1) and (2) have the forms:

$$\mathbf{F} = \frac{\partial \boldsymbol{r}}{\partial \bar{\boldsymbol{r}}} = \frac{\partial \boldsymbol{r}}{\partial \boldsymbol{\xi}}\left(\frac{\partial \bar{\boldsymbol{r}}}{\partial \boldsymbol{\xi}}\right)^{-1} = \mathbf{I} + \frac{\partial \boldsymbol{u}_h}{\partial \boldsymbol{\xi}}\left(\frac{\partial \bar{\boldsymbol{r}}}{\partial \boldsymbol{\xi}}\right)^{-1}, \tag{20}$$
$$\mathbf{R} = \mathbf{R}(\boldsymbol{\theta}(\boldsymbol{\xi})).$$

The internal virtual work W_{int} is given as:

$$\delta W_{\text{int}} = -\int_V \left(\mathbf{t} : \frac{\partial \mathbf{H}}{\partial \boldsymbol{q}} + \mathbf{m} : \frac{\partial \boldsymbol{I}^T}{\partial \boldsymbol{q}}\right) dV \cdot \delta\boldsymbol{q}, \tag{21}$$

and the virtual work of the external forces has the form (Obrezkov et al., 2020):

$$\begin{aligned}\delta W_{\text{ext}} &= \int_V \boldsymbol{b}^T\delta\boldsymbol{r}dV + \int_S \boldsymbol{n}^T\delta\boldsymbol{r}dS \\ &= \left(\int_V \boldsymbol{b}^T\mathbf{N}_m dV + \int_S \boldsymbol{n}^T\mathbf{N}_m dS\right)\cdot\delta\boldsymbol{q},\end{aligned} \tag{22}$$

where vectors $\boldsymbol{b}$ and $\boldsymbol{n}$ are the vector of body and surface forces, respectively. S is the body surface. Assuming that we are dealing with static tasks, we have:

$$\delta W_{\text{ext}} + \delta W_{\text{int}} = 0. \tag{23}$$

Table 1
The deformations in the y direction [m] of the rectangular cantilever beam problem within classic linear elasticity; n is the number of the elements.

n	ANCF Cauchy	ANCF Cosserat	$n_H \times n_W \times n_L$	Solid Cosserat	Solid Cauchy	ANSYS SOLID185
1	0.000655	0.000655	$1\times1\times2$	0.000296	0.000296	0.000398
2	0.000757	0.000757	$2\times2\times4$	0.000548	0.000548	0.000607
4	0.000783	0.000783	$4\times4\times10$	0.000739	0.000739	0.000766
8	0.000793	0.000793	$8\times8\times16$	0.000776	0.000776	0.000786
Reference solution				0.0008099		

4. Numerical results

In this section, we use the derived finite element to analyse a few static problems for solids. To check the results for the ANCF micropolar element, we will compare them with analytical solutions, if any are available, and with the 3D micropolar solid element developed in Eremeyev et al. (2016a) and Eremeyev et al. (2016b), hereinafter called "Solid Cosserat". Its counterpart within the Cauchy theory is called "Solid Cauchy".

4.1. Deformation within linear micropolar elasticity

Here, we consider the solutions obtained within linear micropolar elasticity with the strain relations given in Eq. (8). The reason for dividing cases into linear and non-linear is that most of the work related to micropolar elasticity considers only linear relations. Therefore, these tasks with known solutions, including analytical ones, can be considered as benchmark problems. That allows checking the robustness of the offered calculation scheme. On the contrary, in the non-linear regime, the solutions are not so broadly presented, with only two known papers (Bauer et al., 2010; Erdelj et al., 2020). In the following subsection, these theories will also be compared.

Bending within Cauchy linear elasticity

Firstly, the algorithm will be checked for linear displacements within Cauchy media. For this purpose, we will apply the fact that within linear theory the micropolar elasticity should give the same results as the classic one if microrotations are equal to zero, i.e. assuming $\boldsymbol{\theta} = \mathbf{0}$ or decoupling microrotations and displacements via $N = 0$ (Eremeyev et al., 2016a).

Let us take a rectangular beam: one end of it is fixed, and a vertical force F_y is applied to the free end, as shown in Fig. 2. We take the following set of parameters: $E = 207$ GPa, $\nu = 0.3$, $N = 0$, $l_t = 0.22$ mm, $l_b = 0.45$ mm, $\Psi = 1.5$. E and ν are chosen to follow the bending benchmark problem from Ebel et al. (2017). Other parameters are taken from the work (Eremeyev et al., 2016b), but they do not influence the results, as $N = 0$. F is equal to 62.5×10^3 N. The geometrical dimensions are $l_x = L = 2$ m, $l_y = H = 0.5$ m, $l_z = W = 0.1$ m. Additionally, the convergence rate of the tip displacement is demonstrated in Table 1 as a function of the number of elements n.

As one can see from Table 1, these solutions agree well each other, with the error for ANCF elements equalling 2.1%.

Bending within Cosserat linear elasticity

To show that the developed element works well within micropolar theory as well, we again study the cantilever beam bending problem. However, in this subsection, we consider the bending of two beams with the following geometrical parameters: $L = 0.1016$ m, $W = 0.00762$ m, $H_1 = \frac{L}{20}$, and $H_2 = \frac{L}{10}$. These beams are subjected to the bending load in the y direction $F_y = 4.4482$ N. The physical parameters are $l_t = 0.35921$ mm, $l_b = \frac{l_t}{\sqrt{2}}$, $\Psi = 1$, $N = 0.5$, $\nu = 0.3$, $G = 10.3421$ GPa. These problems were considered in Huang et al. (2000) and provided with finite element solutions based on the Solid Cosserat element, and

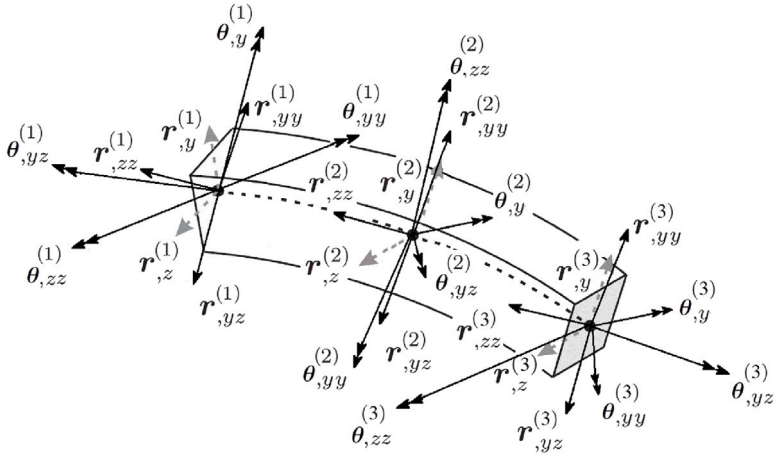

Fig. 1. Illustration of the nodal coordinates for the proposed ANCF Cosserat beam element.

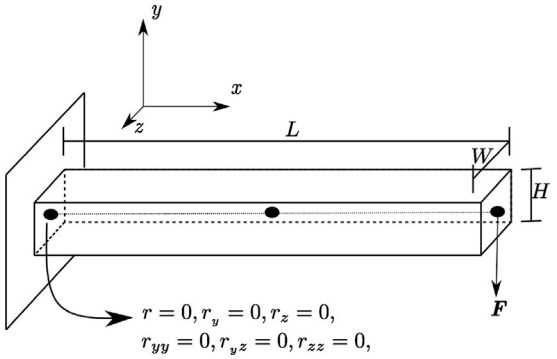

Fig. 2. Geometry and boundary conditions for the bending benchmark within the classic linear elasticity.

Table 2
The deformations in the y direction of the rectangular cantilever beam problems within the micropolar linear elasticity in mm.

n	ANCF Cosserat			
	Beam №1 in [mm]		Beam №2 in [mm]	
	Results	Error (%)	Results	Error (%)
1	4.83399	27.21	0.64088	25.35
2	6.04260	9.004	0.79486	7.410
4	6.40551	3.539	0.83735	2.460
8	6.52729	1.705	0.85049	0.930
16	6.56831	1.087	0.85513	0.389
32	6.58256	0.873	0.85662	0.215
Solid Cosserat (Huang et al., 2000)	6.77926	2.089	0.866648	0.953
Analytic solution (Huang et al., 2000)	6.64052	–	0.85847	–

Table 3
The values of the rotational angle of the microrods varying the cross-section diameter d, with $n = 8$ for ANCF-based solutions.

d in [mm]	ANCF Cauchy	ANCF Cosserat	Solid Cosserat (Tang and Hu, 2017)
4	0.357473	0.07296	0.07279
8	0.049634	0.02198	0.02193
12	0.014734	0.00917	0.00919
24	0.001842	0.00158	0.00158
40	0.000398	0.00037	0.00037
Analytic solution	Difference with the analytic solution of the classical theory (%)		
0.397887	10.157	81.663	81.706
0.049736	0.2051	55.806	55.907
0.014736	0.0136	37.771	37.635
0.001842	0	14.224	14.224
0.000398	0	7.0352	7.0352

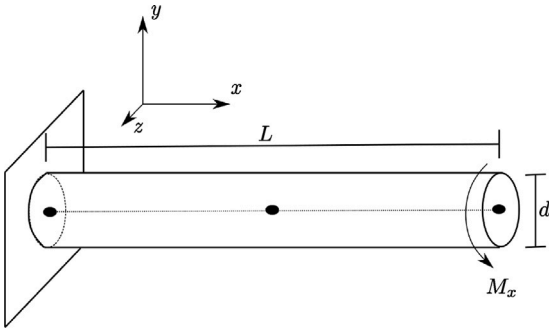

Fig. 3. Setup for the torsion benchmark within the micropolar linear elasticity given in Tang and Hu (2017).

analytical solutions. For easy understanding, all data here are given in the metric system in contrast to the original paper, where they are presented in the imperial one.

As one can see, the numerical solution errors presented in Table 2 for the ANCF Cosserat element in comparison with the analytical results provided by Huang et al. (2000) are 0.9% and 0.2%, respectively. These are less than the errors obtained by the same authors for the solid element: 2.1% and 0.95%, respectively.

Torque of the micropolar beam

Next, we consider a task of the microrod torque, which was previously considered in the work of Tang and Hu (2017). Firstly, we want to point out the different notation is used in the paper. To have it agree with the description given in Section 2, the following changes should be made: $G_c = \frac{\kappa}{2}$, $l_c = l_t = \sqrt{2} l_b$ and $\Psi = 1$. These changes lead to $N = \sqrt{\frac{G_c}{G_c+G}}$, $\alpha = 0$, $\beta = 0$, where G_c and l_c are called the Cosserat shear modulus and internal scale, respectively. However, it should be added that the theory described above is related to the so-called 2D micropolar continuum according to Fantuzzi et al. (2018).

Now, let us consider the cantilever beam with a circular cross-section, as given in Fig. 3. The free end of the beam is subjected to a torque with a magnitude of $M_x = 10$ N m. The length of the rod is given via the relation $\frac{L}{d} = 10$, where d is the diameter of the rod cross-section.

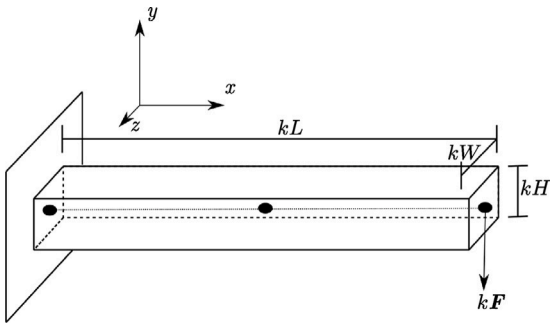

Fig. 4. Setup for the size-effect benchmark within micropolar linear elasticity, with size-coefficient k.

The physical parameters are the following: $G_c = 25$ GPa, $l_c = 2$ mm, Young's modulus $E = 2G(1+\nu)$ and Poisson's ratio of the material are 100 GPa and 0.25, respectively. The constant values are taken from Tang and Hu (2017), and following the paper, we also present an analytical value for the rotational angle at the free end within the classical linear theory.

The variation of the cross-section diameter d leads to the results presented in Table 3.

The number of the used ANCF elements is equal to 8. As one can see, the solutions agree very well with ones presented in Tang and Hu (2017) and suggest the entire algorithm performs well. Moreover, here it is possible to notice the size-effect: the smaller samples are used, the more different the solutions are between the classical and Cosserat theories.

Size-effect prediction Cosserat linear elasticity

Let us consider the size-effect problem in detail. We consider the cantilever bending problem. We take the following physical features: $G = 4000$ MPa, $\nu = 0.25$, $N = 0.5$, $l_t = 0.22$ mm, $l_b = 0.45$ mm, $\Psi = 1.5$. These constants represent micropolar material data for bones (Eremeyev et al., 2016b), with the initial geometrical dimensions $L = 0.03$ m, $H = 0.01$ m, $W = 0.002$ m taken from the same resource. To one end of the beam, we applied force equal to $F = 500$ N. To represent the size-effect, we will proportionally, on some coefficient k, change all sample dimension lengths as well as the applied force, as presented in Fig. 4. It should be noticed that in the linear Cauchy continuum model the coefficient k does not influence on the results.

Table 4
The deformations in the y direction of the rectangular sample with dependency on the size coefficient k.

ANCF Cosserat			
n	k = 0.1	k = 1	k = 10
1	0.00110949	0.00241114	0.00245122
2	0.00135497	0.00272995	0.00277405
4	0.00147545	0.00279695	0.00283931
8	0.00152856	0.00281964	0.00286080
16	0.00155007	0.00282770	0.00286850
32	0.00155706	0.00282995	0.00287086
64	0.00155847	0.00283037	0.00287148
Solid Cosserat			
$n_H \times n_W \times n_L$	k = 0.1	k = 1	k = 10
1 × 1 × 2	0.00075488	0.00122865	0.00124078
2 × 2 × 4	0.00114452	0.00210155	0.00212999
4 × 4 × 8	0.00138504	0.00260418	0.00264265
8 × 8 × 16	0.00149324	0.00278504	0.00282668
10 × 10 × 20	0.00151196	0.00281017	0.00285221
12 × 12 × 24	0.00152361	0.00282444	0.00286670
13 × 13 × 26	0.00152788	0.00282937	0.00287171

The variation of the size-coefficient $k \in [0.1, 10]$ means the varying of the size from $0.003 \leqslant L \leqslant 0.3$ m, $0.001 \leqslant H \leqslant 0.1$ m, and $0.0002 \leqslant W \leqslant 0.02$ m.

As one can see from Table 4, the variation in size may affect the final results of each sample significantly. In Fig. 5(a), we also demonstrate the convergence rate of numerical calculations for several proposed samples, where the relative error is defined as follows.

$$\text{Relative error} = \frac{\|sol_{i+1} - sol_i\|}{sol_{i+1}}, \tag{24}$$

where $\|\cdot\|$ is defined as L_2 norm.

From Fig. 5(b) and Table 4, it is noticeable that two elements show approximately the same results in the full range $k \in [0.1, 10]$, but the ANCF element demonstrates faster convergence, as Fig. 5(a) shows. That proves that the ANCF requires significantly less computational power.

4.2. Non-linear micropolar elasticity

In the literature, the results obtained within the non-linear Cosserat elasticity are barely presented, which can be explained by the computational difficulties during the utilization of the non-linear relations, especially in the cases of computationally heavy micropolar solid elements,

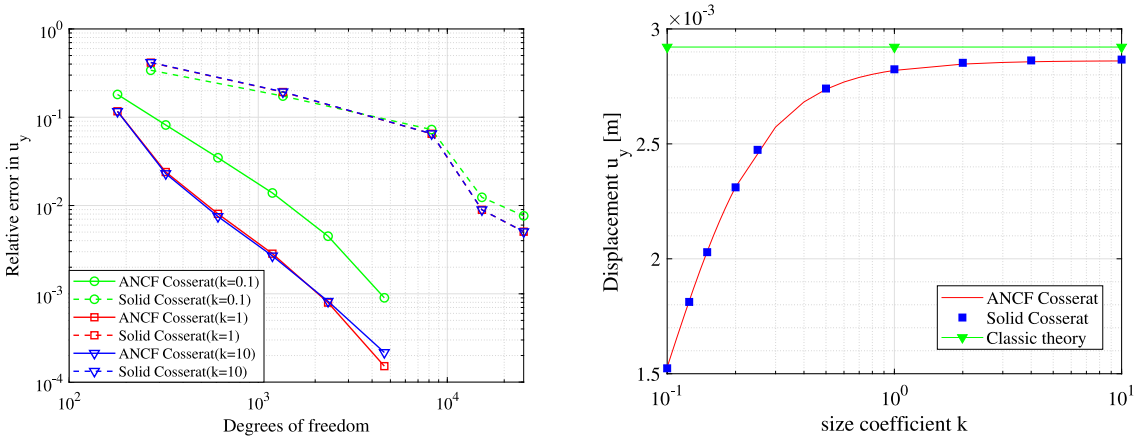

(a) The convergence rate for the samples with different size-coefficient k

(b) The displacement dependency from the size-coefficient k

Fig. 5. Illustration of Table 4, the influence of the size element dependency (coefficient k) on displacements within linear micropolar theory.

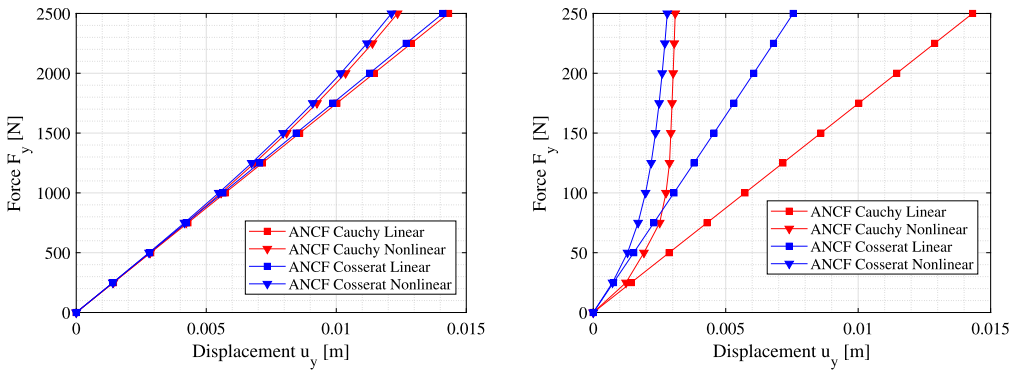

(a) The displacement dependency from the size coefficient $k = 1$

(b) The displacement dependency from the size coefficient $k = 0.1$

Fig. 6. Illustration of the force–displacement linear and non-linear correlations within the Cauchy and Cosserat theories for two beams with size coefficients $k = 0.1$ and $k = 1$.

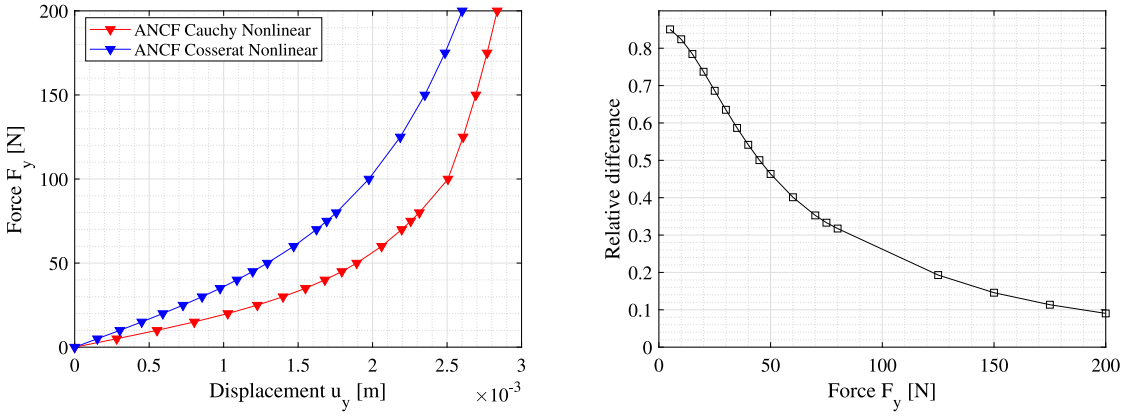

(a) The non-linear force-displacement dependency between the micropolar and classical theories

(b) The relative differences between the micropolar and classical theories for $k = 0.1$

Fig. 7. Illustration of the differences in non-linear behaviour for the cantilever bending problem within the Cauchy and Cosserat theories, for a beam with a size-coefficient equal to $k = 0.1$.

as in the work (Bauer et al., 2010). In Section 4.1, we have already shown the computational efficiency of the ANCF-based micropolar element over the Solid one within the linear Cosserat theory.

Let us consider the task of the cantilever beam bending given above just for two different size coefficients k: $k = 0.1$ and $k = 1$. Here, we analyse the problem both using geometrically linear kinematic relations (8) and using non-linear kinematics (7), (5).

As one can see from Fig. 6, for the larger sample size, the differences between the Cauchy and Cosserat theories are minimal regardless of linear or non-linear theory is applied. At the same time, for the smaller sample, one can notice serious differences in linear theories' predictions, which were shown already in Table 4 and Fig. 5(b). However, the comparison between the non-linear Cauchy and Cosserat theories reveals that initial differences can reduce with the application of further loading.

To present the matter in detail for the smaller samples, let us consider only non-linear theories for the case $k = 0.1$.

From Fig. 7(b) one can notice, the difference might be up to 90% in the initial loading cases, where the relative difference is defined as

$$\text{Relative difference} = \frac{\|sol_{Cosserat} - sol_{Cauchy}\|}{sol_{Cosserat}}. \tag{25}$$

However, under this loading, the displacements might be approximated with linear theory, and for this benchmark, it would be sensible to consider the difference between the non-linear theories when $F_y \geq 50$

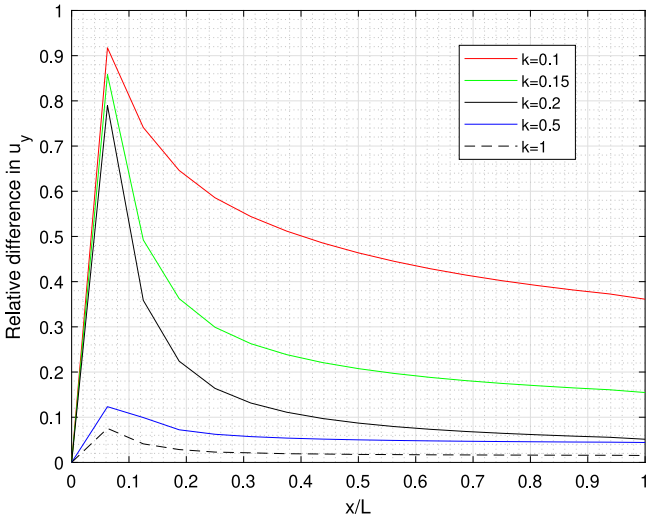

Fig. 8. The relative difference between the non-linear solutions evaluated over the whole beam length under bending load $F_y = 50 \cdot k$.

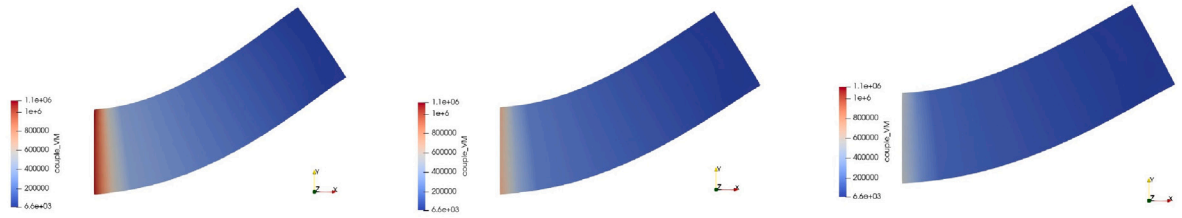

(a) $k = 0.1$ (b) $k = 0.15$ (c) $k = 0.2$

Fig. 9. The von Mises-like couple stress distributions with different size-coefficient k under bending load $F_y = 500 \cdot k$, $L = 0.03 \cdot k$ m, $H = 0.01 \cdot k$ m, $W = 0.002 \cdot k$ m.

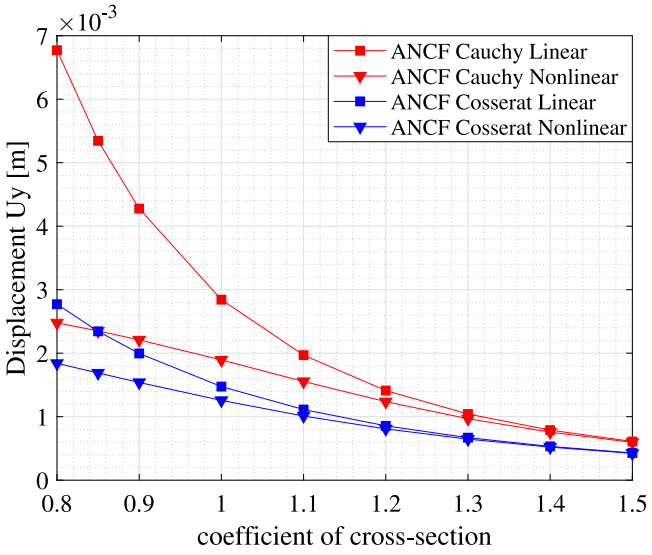

Fig. 10. The displacement dependency from the size-coefficient of the cross-section k_2.

N, where the differences are about 40% with the further tendency to decrease. The closeness of the two theories under large bending loads is because the benchmark task is targeting its bending angle limit under applied force of $\pi/2$, where elongation deformations appear instead of bending.

Comparing further the relative difference theories over the whole beam length for the $F_y = 50 \cdot k$ from Fig. 7, one can obtain the dependencies presented in Fig. 8 for the different size-coefficients.

From Fig. 8 we can see, that the biggest influence is at the fixed edge. Therefore, based on this result and the results presented in Figs. 6 and 7, one can conclude that couple stresses are most intensive at the edge while decreasing with the increase of the size coefficient. To verify that claim, let us consider the couple stress distribution for the size-coefficients $k = 0.1, 0.15, 0.2$. Couple stresses are compared with the von Mises yield criteria as follows.

$$\mathrm{m}_{VM} = \sqrt{\frac{3}{2}(m_{ij} - \frac{1}{3}\mathrm{tr}(\mathbf{m})\delta_{ij})(m_{ij} - \frac{1}{3}\mathrm{tr}(\mathbf{m})\delta_{ij})}. \tag{26}$$

As one can see from Fig. 9, the influence of the couple stress is mostly concentrated at the fixed edge with the decreasing tendency while the size coefficient increasing.

Next, we want to demonstrate the influence of cross-section size. For this reason, we consider the case with size-coefficient $k = 0.1$ and applied load $F_y = 50$ where the influence of non-linearities is the most noticeable. To vary the cross-section, we will proportionally, on some coefficient k_2, change the width and height of the sample, $k \in [0.8, 1.5]$. Therefore, the variation of the cross-section geometrical parameters is $0.0008 \leqslant H \leqslant 0.0015$ m, and $0.00016 \leqslant W \leqslant 0.0003$ m (see Fig. 10).

5. Conclusion

This work has examined beam-like structures within Cosserat continuum. The authors have utilized two FE schemes based on absolute nodal coordinate formulations and solid elements for the analysis, accompanied by analytical solutions. The algorithm for 3D FE was based on the work of Eremeyev et al. (2016a) and has been included for validation purposes and to highlight the computational advantage of the new ANCF beam element. To the best of the authors' knowledge, it was the first attempt to implement micropolar media in a continuum beam formulation within non-linear deformation regime. This work demonstrated the behaviour of the beam-like structures based on the micropolar theory with linear and non-linear stress–strain relationships. The results showed that the ANCF-based results agreed well with ones obtained with the 3D micropolar solid element within the linear Cosserat theory. Moreover, during bending and torsion loading cases, the ANCF element converges closer to the reference solutions than those from the 3D micropolar solid element. Furthermore, the ANCF element converges faster than the solid element. Then, based on two formulations, in graphical and tabular forms, the size-dependency of deformations was shown. Finally, the non-linear effects were presented during bending tests and showed that they matter in some deformation range.

Declaration of competing interest

The authors declare that they have no known competing financial interests or personal relationships that could have appeared to influence the work reported in this paper.

Acknowledgements

We would like to thank the Academy of Finland (Application No. 299033 for funding of Academy Research Fellow) for the generous grant that made this work possible.

References

Aero, E., Kuvshinskii, E.V., 1960. Basic equations of the theory of elasticity with rotational interaction of particles. Phys. Solid State 2 (7), 1399—1409.

Akgöz, B., Civalek, O., 2015. A novel microstructure-dependent shear deformable beam model. Int. J. Mech. Sci. 99, 10–20. http://dx.doi.org/10.1016/j.ijmecsci.2015.05.003.

Atroshchenko, E., Hale, J.S., Videla, J.A., Potapenko, S., Bordas, S.P., 2017. Microstructured materials: Inhomogeneities and imperfect interfaces in plane micropolar elasticity, a boundary element approach. Eng. Anal. Bound. Elem. 83, 195–203. http://dx.doi.org/10.1016/j.enganabound.2017.07.023.

Bauer, S., Schäfer, M., Grammenoudis, P., Tsakmakis, C., 2010. Three-dimensional finite elements for large deformation micropolar elasticity. Comput. Methods Appl. Mech. Engrg. 199 (41), 2643–2654. http://dx.doi.org/10.1016/j.cma.2010.05.002.

Carrera, E., Zozulya, V.V., 2021. Carrera unified formulation (CUF) for the micropolar beams: Analytical solutions. Mech. Adv. Mater. Struct. 28 (6), 583–607. http://dx.doi.org/10.1080/15376494.2019.1578013.

Choi, M.-J., Sauer, R.A., Klinkel, S., 2021. An isogeometric finite element formulation for geometrically exact Timoshenko beams with extensible directors. Comput. Methods Appl. Mech. Engrg. 385, 113993. http://dx.doi.org/10.1016/j.cma.2021.113993.

Cosserat, E., Cosserat, F., 1909. Théorie des Corps déformables. Nature 81, 1399—1409. http://dx.doi.org/10.1038/081067a0.

Ebel, H., Matikainen, M.K., Hurskainen, V.-V., Mikkola, A., 2017. Higher-order beam elements based on the absolut nodal coordinate formulation for three-dimensional elasticity. Nonlinear Dynam. 88, 1075–1091. http://dx.doi.org/10.1007/s11071-016-3296-x.

Engel, U., Eckstein, R., 2002. Microforming—from basic research to its realization. J. Mater Process. Technol. 125–126, 35–44. http://dx.doi.org/10.1016/S0924-0136(02)00415-6.

Erdelj, S.G., Jelenić, G., Ibrahimbegović, A., 2020. Geometrically non-linear 3D finite-element analysis of micropolar continuum. Int. J. Solids Struct. 202, 745–764. http://dx.doi.org/10.1016/j.ijsolstr.2020.05.025.

Eremeyev, V., Lebedev, L., Altenbach, H., 2013. Foundations of Micropolar Mechanics. Springer, Berlin, Heidelberg, http://dx.doi.org/10.1007/978-3-642-28353-6.

Eremeyev, V.A., Skrzat, A., 2017. Linear micropolar elasticity analysis of stresses in bones under static loads. Strength Mater. 49, 575–585. http://dx.doi.org/10.1007/s11223-017-9901-5.

Eremeyev, V.A., Skrzat, A., Stachowicz, F., 2016a. On finite element computations of contact problems in micropolar elasticity. Adv. Mater. Sci. Eng. 1–9. http://dx.doi.org/10.1155/2016/9675604.

Eremeyev, V., Skrzat, A., Vinakurava, A., 2016b. Application of the micropolar theory to the strength analysis of bioceramic materials for bone reconstruction. Strength Mater. 48, 573–582. http://dx.doi.org/10.1007/s11223-016-9800-1.

Ericksen, J.L., Truesdell, C., 1957. Exact theory of stress and strain in rods and shells. Arch. Ration. Mech. Anal. 1, 295–323. http://dx.doi.org/10.1007/BF00298012.

Eringen, A.C., 1967. Linear theory of micropolar viscoelasticity. Internat. J. Engrg. Sci. 5 (2), 191–204. http://dx.doi.org/10.1016/0020-7225(67)90004-3.

Eringen, A.C., 1999. Microcontinuum Field Theories, Vol. 1. Springer, http://dx.doi.org/10.1007/978-1-4612-0555-5.

Eringen, A.C., Kafadar, C., 1976. Part I. Polar Field Theories, Vol. 4. Continuum Physics.

Fantuzzi, N., Leonetti, L., Trovalusci, P., Tornabene, F., 2018. Some novel numerical applications of cosserat continua. Int. J. Comput. Methods 15 (06), 1850054. http://dx.doi.org/10.1142/S0219876218500548.

Hassanpour, S., Heppler, G., 2016. Comprehensive and easy-to-use torsion and bending theories for micropolar beams. Int. J. Mech. Sci. 114, 71–87. http://dx.doi.org/10.1016/j.ijmecsci.2016.05.007.

Hassanpour, S., Heppler, G.R., 2017. Micropolar elasticity theory: a survey of linear isotropic equations, representative notations, and experimental investigations. Math. Mech. Solids 22, 224–242. http://dx.doi.org/10.1177/1081286515581183.

Huang, F.-Y., Yan, B.-H., Yan, J.-L., Yang, D.-U., 2000. Bending analysis of micropolar elastic beam using a 3–D finite element method. Internat. J. Engrg. Sci. 38, 275–286. http://dx.doi.org/10.1016/S0020-7225(99)00041-5.

Kafadar, C., Eringen, A.C., 1971a. Micropolar media—I the classical theory. Internat. J. Engrg. Sci. 9 (3), 271–305. http://dx.doi.org/10.1016/0020-7225(71)90040-1.

Kafadar, C., Eringen, A.C., 1971b. Micropolar media—II the relativistic theory. Internat. J. Engrg. Sci. 9, 307–329. http://dx.doi.org/10.1016/0020-7225(71)90041-3.

Kiani, K., 2017. Large deformation of uniaxially loaded slender microbeams on the basis of modified couple stress theory: Analytical solution and Galerkin-based method. Physica E 93, 301–312.

Krishnaswamy, S., 1996. A Cosserat-type model for the red blood cell wall. Internat. J. Engrg. Sci. 34 (8), 873–899. http://dx.doi.org/10.1016/0020-7225(95)00139-5.

Lakes, R.S., 1983. Size effects and micromechanics of a porous solid. J. Mater. Sci. 18, 2572–2580. http://dx.doi.org/10.1007/BF00547573.

Lakes, R.S., 1986. Experimental microelasticity of two porous solids. Int. J. Solids Struct. 22, 55–63. http://dx.doi.org/10.1016/0020-7683(86)90103-4.

Lakes, R., 1995. Experimental methods for study of cosserat elastic solids and other generalized elastic continua. In: Continuum Models for Materials with Micro-Structure. pp. 1–22.

Liu, X., Zhao, S., Qin, Y., Nawang, W.A.W., 2015. Influence of size effects on material properties and springback behavior of metal foils in micro bending: A review. MATEC Web Conf. 21, 09010. http://dx.doi.org/10.1051/matecconf/20152109010.

Münch, I., Neff, P., Wagner, W., 2011. Transversely isotropic material: nonlinear Cosserat versus classical approach. Contin. Mech. Thermodyn. 23, 27–34. http://dx.doi.org/10.1007/s00161-010-0150-0.

Nachbagauer, K., 2014. State of the art of ANCF elements regarding geometric description, interpolation strategies, definition of elastic forces, validation and the locking phenomenon in comparison with proposed beam finite element. Arch. Comput. Methods Eng. 21, 293–319. http://dx.doi.org/10.1007/s11831-014-9117-9.

Nampally, P., Reddy, J.N., 2020. Geometrically nonlinear Euler–Bernoulli and Timoshenko micropolar beam theories. Acta Mech. 231, 4217–4242. http://dx.doi.org/10.1007/s00707-020-02764-x.

Neff, P., Jeong, J., 2009. A new paradigm: the linear isotropic cosserat model with conformally invariant curvature energy. ZAMM - J. Appl. Math. Mech. / Z. Angew. Math. Mech. 89 (2), 107–122. http://dx.doi.org/10.1002/zamm.200800156.

Neff, P., Jeong, J., Fischle, A., 2010. Stable identification of linear isotropic cosserat parameters: Bounded stiffness in bending and torsion implies conformal invariance of curvature. Acta Mech. 211, 237–249. http://dx.doi.org/10.1007/s00707-009-0230-z.

Obrezkov, L.P., Eliasson, P., Harish, A.B., Matikainen, M.K., 2021. Usability of finite elements based on the absolute nodal coordinate formulation for the achilles tendon modelling. Int. J. Non-Linear Mech. 129, 103662. http://dx.doi.org/10.1016/j.ijnonlinmec.2020.103662.

Obrezkov, L.P., Matikainen, M.K., Harish, A.B., 2020. A finite element for soft tissue deformation based on the absolute nodal coordinate formulation. Acta Mech. 231, 1519–1538. http://dx.doi.org/10.1007/s00707-019-02607-4.

Obrezkov, L.P., Mikkola, A., Matikainen, M.K., 2022. Performance review of locking alleviation methods for continuum ANCF beam elements. Nonlinear Dynam. 109, 531–546. http://dx.doi.org/10.1007/s11071-022-07518-z.

Pabst, W., 2005. Micropolar materials. Ceram. Silik. 49, 170–180.

Park, H.C., Lakes, R.S., 1986. Cosserat micromechanics of human bone: Strain redistribution by a hydration sensitive constituent. J. Biomech. 19 (5), 385–397. http://dx.doi.org/10.1016/0021-9290(86)90015-1.

Pietraszkiewicz, W., Eremeyev, V., 2009. On vectorially parameterized natural strain measures of the non-linear Cosserat continuum. Int. J. Solids Struct. 46 (11), 2477–2480. http://dx.doi.org/10.1016/j.ijsolstr.2009.01.030.

Providas, E., Kattis, M., 2002. Finite element method in plane Cosserat elasticity. Comput. Struct. 80, 2059–2069. http://dx.doi.org/10.1016/S0045-7949(02)00262-6.

Ramezani, S., Naghdabadi, R., 2007. Energy pairs in the micropolar continuum. Int. J. Solids Struct. 44 (14), 4810–4818. http://dx.doi.org/10.1016/j.ijsolstr.2006.12.006.

Ramezani, S., Naghdabadi, R., 2010. Micropolar hypo-elasticity. Arch. Appl. Mech. 80, 1449–1461. http://dx.doi.org/10.1007/s00419-010-0466-z.

Ramezani, S., Naghdabadi, R., Sohrabpour, S., 2009. Constitutive equations for micropolar hyper-elastic materials. Int. J. Solids Struct. 46 (14), 2765–2773. http://dx.doi.org/10.1016/j.ijsolstr.2008.10.009.

Reddy, J., 2011. Microstructure dependent couple stress theories of functionally graded beams. J. Mech. Phys. Solids 59, 2382–2399. http://dx.doi.org/10.1016/j.jmps.2011.06.008.

Rhim, J., Lee, S.W., 1998. A vectorial approach to computational modelling of beams undergoing finite rotations. Internat. J. Numer. Methods Engrg. 41, 527–540. http://dx.doi.org/10.1002/(SICI)1097-0207(19980215)41:3<527::AID-NME297>3.0.CO;2-7.

Riahi, A., Curran, J.H., 2009. Full 3D finite element cosserat formulation with application in layered structures. Appl. Math. Model. 33 (8), 3450–3464. http://dx.doi.org/10.1016/j.apm.2008.11.022.

Romero, I., 2008. A comparison of finite elements for nonlinear beams: The absolute nodal coordinate and geometrically exact formulations. Multibody Syst. Dyn. 20, 51–68. http://dx.doi.org/10.1007/s11044-008-9105-7.

Shabana, A.A., 1997. Definition of the slopes and the finite element absolute nodal coordinate formulation. Multibody Syst. Dyn. 1, 339–348. http://dx.doi.org/10.1023/A:1009740800463.

Surana, K., Joy, A., Reddy, J., 2017. Non-classical continuum theory for solids incorporating internal rotations and rotations of Cosserat theories. Contin. Mech. Thermodyn. 29, 665–698. http://dx.doi.org/10.1007/s00161-017-0554-1.

Tang, H.X., Hu, Z.L., 2011. Three dimensional Cosserat continuum model and its application to analysis for the Cantilever beam. Appl. Mech. Mater. 117–119, 438–442. http://dx.doi.org/10.4028/www.scientific.net/AMM.117-119.438.

Tang, H.-X., Hu, Z.-L., 2017. Application of the Cosserat continua to numerical studies on the properties of the materials. Mech. Adv. Mater. Struct. 24 (10), 797–808. http://dx.doi.org/10.1080/15376494.2016.1196784.

Trovalusci, P., Masiani, R., 2003. Non-linear micropolar and classical continua for anisotropic discontinuous materials. Int. J. Solids Struct. 40, 1281–1297. http://dx.doi.org/10.1016/S0020-7683(02)00584-X.

Truesdell, C.A., Noll, W., 1965. The Non-Linear Field Theories of Mechanics, Vol. 3. Springer, Berlin.

Walsh, S.D.C., Tordesillas, A., 2006. Finite element methods for micropolar models of granular materials. Appl. Math. Model. 30 (10), 1043–1055. http://dx.doi.org/10.1016/j.apm.2005.05.016.

Yang, F., Chong, A., Lam, D., Tong, P., 2002. Couple stress based strain gradient theory for elasticity. Int. J. Solids Struct. 39 (10), 2731–2743. http://dx.doi.org/10.1016/S0020-7683(02)00152-X.